

# Symmetry sustained valley-pseudospin textures of the full-zone excitonic bands of transition-metal dichalcogenide monolayers

Ping-Yuan Lo,<sup>1</sup> Guan-Hao Peng,<sup>1</sup> Wei-Hua Li,<sup>1</sup> Yi Yang,<sup>1</sup> and Shun-Jen Cheng<sup>1</sup>

<sup>1</sup>*Department of Electrophysics, National Chiao Tung University, Hsinchu 300, Taiwan*

## Abstract

Preserving high degree of valley polarization of photo-excited excitons in transition-metal dichalcogenide monolayers (TMD-MLs) is desirable for the valley-based photonic applications, but widely recognized as a hard task hindered by the intrinsic electron-hole exchange interaction. In this study, we present a comprehensive investigation of valley-polarized finite-momentum excitons in WSe<sub>2</sub>-MLs over the entire Brillouin zone by solving the density-functional-theory(DFT)-based Bethe-Salpeter equation (BSE) under the guidance of symmetry analysis. We reveal that finite-momentum excitons are generally well immune from the exchange-induced valley depolarization, except for those with specific exciton momenta directionally coincide with the axes associated with the  $3\sigma_v$  and  $3C'_2$  symmetries in TMD-MLs. Sustained by the symmetries, the valley pseudo-spin texture of the full-zone exciton band in the momentum space is locally featured by individual skyrmion-like structures where highly valley-polarized finite-momentum exciton states are centred. Furthermore, we show that, under the assistance of phonons, the high degree of valley polarizations of the finite-momentum exciton states are excellently very well transferable to the optical polarization of the resulting indirect photo-luminescence.

PACS numbers:

*Introduction*— Transition-metal dichalcogenide monolayers (TMD-MLs) have drawn a broad interest in recent years because of the intriguing spin-valley-coupled characteristics in the electronic and excitonic structures [1–3]. As a massive Dirac material, the band structure of a TMD-ML is characterized by two distinctive gapped valleys locating at the  $K$  and  $K'$  corners of the first Brillouin zone (BZ) in the momentum space that follow the distinct optical selection rules and allow for the valley-selective excitation and coherent control by optical helicity [4–6]. Those spin- and valley-resolvable characteristics in the excitonic structure of TMD-MLs serve as a prospective base of spin- and valley-based photonics, as long as a high degree of the excitonic valley polarization can be well maintained in the materials.[7, 8]

However, in reality, the valley-polarization of bright excitons in TMD-MLs are very likely to be depolarized by the electron-hole ( $e$ - $h$ ) exchange interaction which intrinsically couples two interband excitations in distinct valleys [4, 9–12]. Despite the weak coupling strength of meV scale, the  $e$ - $h$  exchange interaction can intermix the distinct spin-like exciton states *completely* whenever the uncoupled exchange-free exciton states possess the same momentum and same energy, which together facilitate the resonant coupling driven by the momentum-conserving exchange interaction.[4, 13] Such a resonant inter-valley coupling exists in the bright exciton with nearly vanishing momentum but, without the sustain from certain symmetries, is not necessary to be held by a generic exciton with finite exciton wave vector,  $\mathbf{k}_{ex} \neq 0$ .

In spite of violating the optical selection rules, the finite-momentum exciton states of TMD-MLs have been shown observable in advanced optical spectroscopies and essentially involved in various optical phenomena e.g. the phonon- or defect-assisted luminescences [14–18], formation of multi-exciton complexes [19], the boost of near-field energy transfers [20] and the optical responses in electron energy loss spectroscopy (EELS) spectroscopy. [21, 22] To understand the exciton physics in TMD-MLs comprehensively, it is demanded to acquire the complete information of the exciton band structures over the entire BZ, which however has not been fully revealed so far.[23–25]

In this Letter, we present theoretical and computational studies of the full-zone exciton bands of WSe<sub>2</sub>-MLs by means of the group theory analysis and numerically solving the DFT-based BSE for neutral exciton. The quantum nature of the valley-polarized exciton states as a function of exciton momentum over the BZ is visualized by the valley pseudo-spin texture, where the skyrmion-like structures around highly valley-polarized exciton states are

revealed. Interestingly, the near unity valley polarization of the low-lying finite momentum exciton states is highly converted into the optical polarization through the indirect phonon-assisted photo-luminescences. [14–16]

*Theoretical analysis and numerical methodology*— First, we consider the exciton states with the well-defined center-of-mass wave vector  $\mathbf{k}_{ex}$ ,  $|S, \mathbf{k}_{ex}\rangle = \frac{1}{\sqrt{\mathcal{A}}} \sum_{v\mathbf{c}\mathbf{k}} A_{S, \mathbf{k}_{ex}}(v\mathbf{c}\mathbf{k}) \hat{c}_{c, \mathbf{k}+\mathbf{k}_{ex}}^\dagger \hat{h}_{v, -\mathbf{k}}^\dagger |GS\rangle$  written as a linear combination of the configurations of the electron-hole ( $e$ - $h$ ) pairs,  $\hat{c}_{c, \mathbf{k}+\mathbf{k}_{ex}}^\dagger \hat{h}_{v, -\mathbf{k}}^\dagger |GS\rangle$ , where the particle operator  $\hat{c}_{c, \mathbf{k}}^\dagger$  ( $\hat{h}_{v, -\mathbf{k}}^\dagger$ ) is defined to create the electron (hole) of the wave vector  $\mathbf{k}$  ( $-\mathbf{k}$ ) in the conduction band  $c$  (corresponding to the missing state at  $\mathbf{k}$  in the filled valence band  $v$ ) from acting the ground state of the system with the fully filled valence bands  $|GS\rangle$ ,  $S$  is the index of the exciton band,  $A_{S, \mathbf{k}_{ex}}(v\mathbf{c}\mathbf{k})$  is the amplitude of the  $e$ - $h$  configuration  $\hat{c}_{c, \mathbf{k}+\mathbf{k}_{ex}}^\dagger \hat{h}_{v, -\mathbf{k}}^\dagger |GS\rangle$  in the exciton wave function, and  $\mathcal{A}$  is the area of the 2D material. Throughout this work, our study is focussed on the spin-like exciton states with the same particle spin in the  $c$ - and  $v$ -bands that could be luminescent with the assistance of phonon- or defect-scatterings. The exciton wave function in the reciprocal  $\mathbf{k}$ -space,  $A_{S, \mathbf{k}_{ex}}(v\mathbf{c}\mathbf{k})$ , follows the Bethe-Salpeter equation that reads [23, 25–29]

$$\begin{aligned} & [\epsilon_{c, \mathbf{k}+\mathbf{k}_{ex}} - \epsilon_{v, \mathbf{k}} - E_{S, \mathbf{k}_{ex}}^X] A_{S, \mathbf{k}_{ex}}(v\mathbf{c}\mathbf{k}) \\ & + \sum_{v'c'\mathbf{k}'} U_{\mathbf{k}_{ex}}(v\mathbf{c}\mathbf{k}, v'c'\mathbf{k}') A_{S, \mathbf{k}_{ex}}(v'c'\mathbf{k}') = 0, \end{aligned} \quad (1)$$

where  $E_{S, \mathbf{k}_{ex}}^X$  is the eigen energy of the exciton state, the first two terms on the left hand side are associated with the kinetic energy of a free  $e$ - $h$  pair composed of the kinetic energies of the conduction electron and valence hole,  $\epsilon_{c, \mathbf{k}+\mathbf{k}_{ex}}$  and  $(-\epsilon_{v, \mathbf{k}})$ , and the last term is the kernel of the  $e$ - $h$  Coulomb interaction consisting of the screened  $e$ - $h$  direct and the  $e$ - $h$  exchange ones,  $U_{\mathbf{k}_{ex}} = -V_{\mathbf{k}_{ex}}^d + V_{\mathbf{k}_{ex}}^x$ . In this work, we consider the Coulomb screening on the base of Keldysh formalism [23, 30, 31]. The definitions of  $V_{\mathbf{k}_{ex}}^d$  and  $V_{\mathbf{k}_{ex}}^x$  in terms of the Bloch wave functions are explicitly given in Supplementary Materials [32].

In this work, we set up the BSE theory on the first principles base following the methodology established in Ref. [29]. In the approach, the BSE is formulated in the Wannier tight binding model by means of wannierization of the DFT-calculated Bloch wave functions. Figure 1c presents the DFT-calculated lowest conduction and topmost valence band of a WSe<sub>2</sub>-ML over the first BZ by using the first principles VASP package [33] with the use of the Perdew–Burke–Ernzerhof (PBE) exchange-correlation functional [34]. To solve the

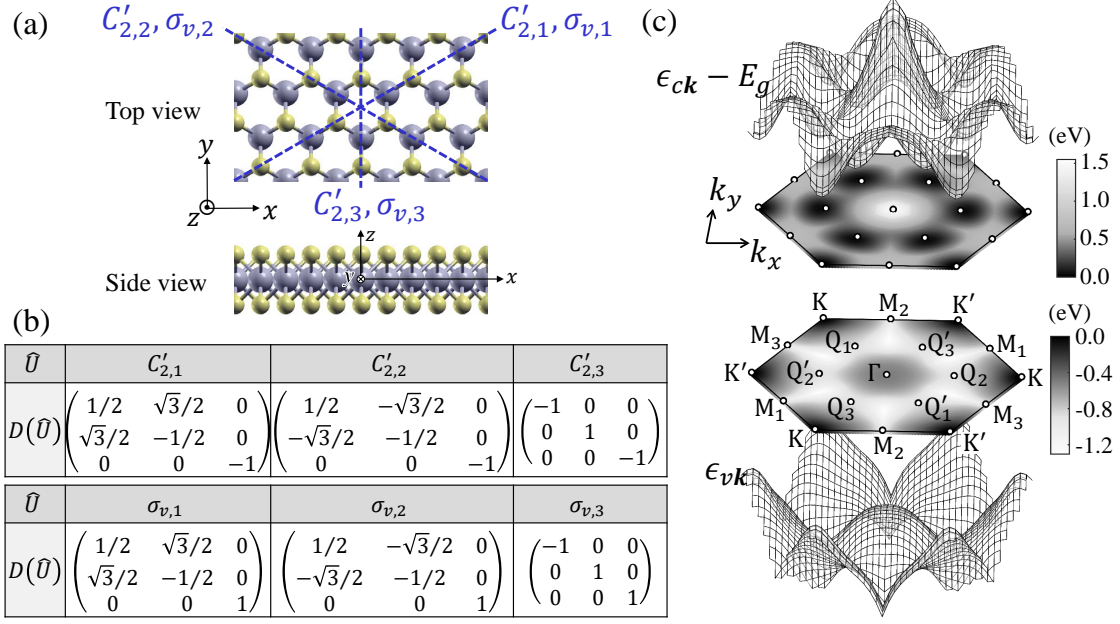


FIG. 1: (a) Top and side views of the crystalline lattice structure of a TMD-ML with  $D_{3h}$  symmetry, where the axes of the  $C'_{2,i}$  rotational symmetry and  $\sigma_{v,i}$  mirror symmetry relevant to the symmetry analysis are indicated by the dashed lines. (b) List of the matrices of the  $C'_{2,i}$  and  $\sigma_{v,i}$  symmetry operators in the Cartesian coordinate. (c) Contour plots of the DFT-calculated lowest conduction (top) and highest valence bands (bottom) of a WSe<sub>2</sub>-ML over the first BZ with the indication of the high symmetry points, where  $E_g$  is used to indicate the energy gap of a WSe<sub>2</sub>-ML.

exciton band structures, the DFT-based BSE is discretized with the  $\mathbf{k}$  mesh grids compatible to the symmetries of  $D_{3h}$  TMD-MLs [25] and solved numerically by means of direct diagonalization.

It is well established that the direct Coulomb interaction makes the predominant contribution to the large binding energy of exciton at the scale of hundreds of meV, but has no direct effect on the coupling between the distinct spin-like exciton states belonging to the opposite valleys [35, 36]. By contrast, the momentum-conserving  $e$ - $h$  exchange interaction at the scale of merely meV could couple the distinct valley-excitons which possess the same exciton momentum  $\mathbf{k}_{ex}$  and leads to the unwanted valley-depolarization of exciton by the valley-based applications [9, 10]. In fact, the valley-intermixing of excitons is significant only when the exchange-free valley-polarized states are degenerate or nearly degenerate where the energy difference must be much smaller than the meV-scaled  $e$ - $h$  exchange interaction.

Thus, we proceed with the symmetry analysis for the finite-momentum exchange-

free electron-hole-pair states over the first BZ to derive the condition for the formation of the valley-degeneracy of the excitation states of  $D_{3h}$  TMD-MLs, where  $D_{3h} = \{E, C_3, C_3^{-1}, \sigma_h, S_3, S_3^{-1}, C'_{2,1}, C'_{2,2}, C'_{2,3}, \sigma_{v,1}, \sigma_{v,2}, \sigma_{v,3}\}$ . [37]

Consider two distinct electron-hole pair states with the same  $\mathbf{k}_{ex}$  excited from the different valence states at  $\mathbf{k}$  and  $\mathbf{k}'$ , respectively, the degeneracy is formed if  $\epsilon_{c,\mathbf{k}+\mathbf{k}_{ex}} - \epsilon_{v,\mathbf{k}} = \epsilon_{c,\mathbf{k}'+\mathbf{k}_{ex}} - \epsilon_{v,\mathbf{k}'}$ , which can generally hold only if  $\epsilon_{v,\mathbf{k}} = \epsilon_{v,\mathbf{k}'}$  and  $\epsilon_{c,\mathbf{k}+\mathbf{k}_{ex}} = \epsilon_{c,\mathbf{k}'+\mathbf{k}_{ex}}$ . From the theory of group representations, the above two equations hold when the space group symmetry of the TMD-ML satisfies both  $\mathbf{k}' = \hat{U}\mathbf{k}$  and  $\mathbf{k}' + \mathbf{k}_{ex} = \hat{U}(\mathbf{k} + \mathbf{k}_{ex})$  for any symmetry operator  $\hat{U} \in D_{3h}$ . Accordingly, we find the criterion for the formation of valley-degeneracy of two distinct  $e$ - $h$  pairs carrying the same  $\mathbf{k}_{ex}$  is given by

$$\mathbf{k}_{ex} = \hat{U}\mathbf{k}_{ex}. \quad (2)$$

The matrix representation of  $\hat{U} \in D_{3h}$  in the Cartesian coordinate, denoted by  $D(\hat{U})$  which serves as the transformation matrix acting on  $\mathbf{k}$ -vectors, are given in Supplementary Materials [32] and, for  $C'_{2,i}$  and  $\sigma_{v,i}$  symmetries, tabulated in Fig. 1b.

Applying all the symmetry operators  $\hat{U}$  onto Eq. (2) for all  $\mathbf{k}_{ex} \in \text{BZ}$ , one can show that the valley  $e$ - $h$  pair states degenerate only when  $\mathbf{k}_{ex}$  lies at the axes connecting  $\Gamma_{ex}$  and  $M_{ex,i}$  points where the vertical planes of the mirror symmetry  $3\sigma_v$  and the  $x-y$  plane intersect, as shown in Fig. 1a. This predicts the impactive valley depolarization in the exciton with the momentum in coincidence with the  $\overline{\Gamma_{ex}M_{ex,i}}$  paths, including the commonly known bright exciton around the  $\Gamma_{ex}$  point [9, 10]. Fig. 2 b and f depict the BZ in the  $\mathbf{k}_{ex}$ -space with the indication of the relevant high-symmetry points.

*Results*— As an illustrative instance, Fig. 2a-d exemplify the two distinctive  $e$ - $h$  pair excitations with the same  $\mathbf{k}_{ex}$  along the  $k_y$ -direction, i.e. the  $\overline{\Gamma_{ex}M_{ex,2}}$ -axis, which are excited from the valence  $K$  to the conduction  $Q'_2$  valleys (red arrow line) and from the valence  $K'$  to the conduction  $Q_2$  valleys (blue arrow line), respectively. The two free excitations are presented in the DFT-calculated quasi-particle band structures of Fig. 2 c and d, and their transition energies are identified to be the same. For comparative illustration, we consider another set of two inter-band transitions excited from the distinctive valence valleys with the common  $\mathbf{k}_{ex}$  along  $\overline{\Gamma_{ex}K'_{ex}}$ , as shown in Fig. 2e-h. With the misaligned  $\mathbf{k}_{ex}$  from  $\overline{\Gamma_{ex}M_{ex,i}}$  the transition energies of the two  $e$ - $h$  pair excitations are no longer degenerate as identified in Figure 2g and h, as predicted by the symmetry analysis.

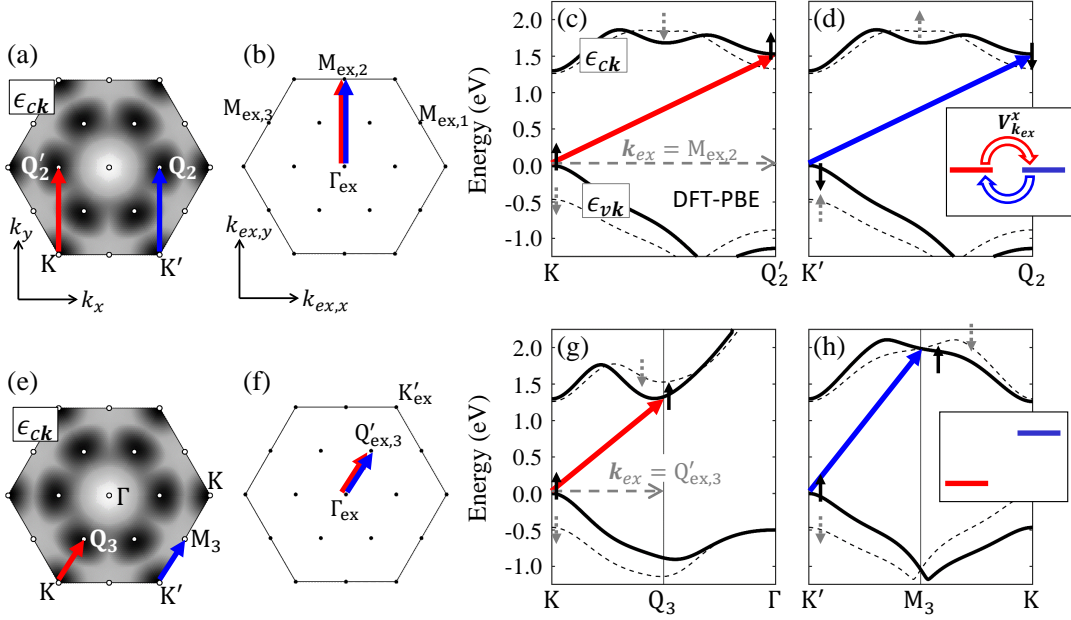


FIG. 2: (a) Two distinct electron-hole pair excitations with the same  $\mathbf{k}_{ex}$  (directed along  $\overline{\Gamma_{ex}M_{ex,2}}$ ), excited from the valence  $K$  to the conduction  $Q'_2$  valleys (red arrow line) and from the valence  $K'$  to the  $Q_2$  conduction valleys (blue arrow line), respectively. (b) The BZ in the exciton-momentum space with the indication of the two excitations. (c) [(d)] The DFT-calculated quasi-particle band dispersion along the momentum direction of the first [second] excitation. Arrow lines indicates the spin-like excitations. (e)-(h): same as the graphs of (a)-(d) but for another set of distinct excitations with the common  $\mathbf{k}_{ex} \parallel \overline{\Gamma_{ex}Q'_{ex,3}}$ . The inset of (d) [(h)] illustrates the existence [absence] of the resonant inter-valley coupling between the two degenerate [non-degenerate] valley-excitations in (a) [(e)].

Beyond the non-interacting  $e$ - $h$  pair states, the symmetry analysis above remains valid for the exchange-free exciton states. Figure 3a shows the calculated energy band dispersions of exchange-free exciton,  $E_{S,\mathbf{k}_{ex}}^{X(0)}$ , with the  $\mathbf{k}_{ex}$  along  $\overline{\Gamma_{ex}M_{ex,2}}$  and  $\overline{\Gamma_{ex}K'_{ex}}$  directions, solved from the exchange-free BSE including the direct part of Coulomb interaction only. In the absence of  $e$ - $h$  exchange interaction, the energy bands of the lowest exciton doublet along  $\overline{\Gamma_{ex}M_{ex,2}}$  does remain degenerate while the ones along  $\overline{\Gamma_{ex}K'_{ex}}$  are shown valley-split in energy. Figure 3b presents the energy splitting of the lowest exchange-free spin-like exciton doublet ( $S = +/ -$  stands for the upper/lower band),  $\Delta_{+-}(\mathbf{k}_{ex}) \equiv E_{+,\mathbf{k}_{ex}}^X - E_{-,\mathbf{k}_{ex}}^X$ , as a function of  $\mathbf{k}_{ex}$  over the BZ, showing the vanishing splitting (indicated by magenta lines) of

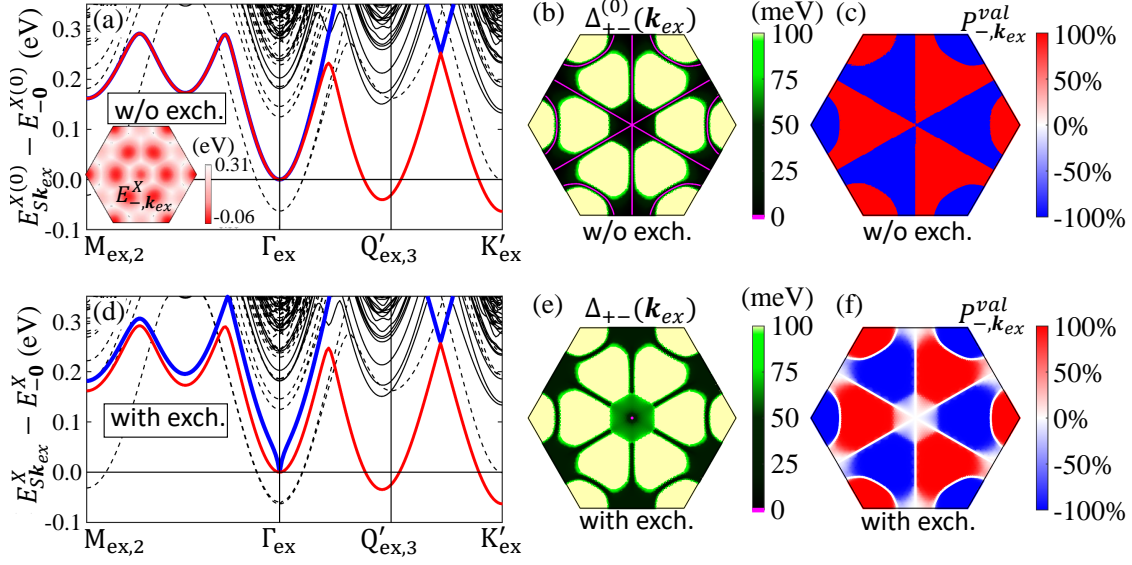


FIG. 3: (a) Exciton band structure calculated with the neglect of the  $e$ - $h$  exchange interaction along the paths of  $\overline{\Gamma_{ex}M_{ex,2}}$  and  $\overline{\Gamma_{ex}Q'_{ex,3}K'_{ex}}$ . Solid (dashed) lines: spin-like (-unlike) exciton bands. Red (blue) curves: the lower (upper) band  $|-, \mathbf{k}_{ex}\rangle$  ( $|+, \mathbf{k}_{ex}\rangle$ ) of the lowest spin-like exciton doublet. Inset: the energy-contour plot of the lowest spin-like exciton band. (b) Contour plot of the energy differences between the lowest spin-like exciton doublet,  $\Delta_{+-}(\mathbf{k}_{ex}) \equiv E_{+, \mathbf{k}_{ex}}^X - E_{-, \mathbf{k}_{ex}}^X$ , over the BZ in the exciton-momentum space. The magenta-coloured line indicates the vanishing splitting ( $\Delta_{+-}(\mathbf{k}_{ex}) = 0$ ). (c) Contour plot of the valley polarization,  $P_{-, \mathbf{k}_{ex}}^{val}$ , of the lowest spin-like exciton states over the BZ. (d)-(f) same as the graphs of (a)-(c) but under the *full* consideration of both direct and exchange Coulomb interaction.

the exchange-free exciton states indeed happening on the three  $\overline{\Gamma_{ex}M_{ex,i}}$  axes.

Figure 3d and e shows the calculated exciton bands and the energy difference between the lowest spin-like doublet of WSe<sub>2</sub>-ML, respectively, with the *full* consideration of the both  $e$ - $h$  direct and exchange interactions. Under the influence of  $e$ - $h$  exchange interaction, the exciton band along the  $\overline{\Gamma_{ex}M_{ex,i}}$  path is no longer degenerate. Writing a valley-mixed exciton state as  $|S, \mathbf{k}_{ex}\rangle = \sum_{\tau=K, K'} \alpha_{S, \mathbf{k}_{ex}}^{\tau} |\tau, \mathbf{k}_{ex}\rangle$ , a linear combination of the exchange-free states with the well-defined valley character,  $\{|\tau, \mathbf{k}_{ex}\rangle\}$ , the degree of valley polarization of the state is measured by  $P_{S, \mathbf{k}_{ex}}^{val} \equiv \frac{|\alpha_{S, \mathbf{k}_{ex}}^K|^2 - |\alpha_{S, \mathbf{k}_{ex}}^{K'}|^2}{|\alpha_{S, \mathbf{k}_{ex}}^K|^2 + |\alpha_{S, \mathbf{k}_{ex}}^{K'}|^2}$ . Accompanied by the exchange-induced splittings, the exciton states lying on the  $\overline{\Gamma_{ex}M_{ex,i}}$  path turn out to be fully valley-mixed and featured by  $P_{-, \mathbf{k}_{ex}}^{val} \sim 0$ , as one can see Fig. 3f in comparison with Fig. 3c. By contrast, the exciton states lying apart from the  $\overline{\Gamma_{ex}M_{ex,i}}$  paths such as those around  $Q_{ex,i}/Q'_{ex,i}$  and

$K_{ex}/K'_{ex}$  valleys yet well maintain the superior high degrees of the valley polarizations with  $|P_{-, \mathbf{k}_{ex}}^{val}| \lesssim 100\%$ .

To further recognize the quantum nature of the valley-polarized exciton states, let us express the numerically calculated lowest exciton states (with the band index of  $S = -$ ),  $|S, \mathbf{k}_{ex}\rangle = -e^{-i\phi_{S, \mathbf{k}_{ex}}} \sin \frac{\theta_{S, \mathbf{k}_{ex}}}{2} |K, \mathbf{k}_{ex}\rangle + \cos \frac{\theta_{S, \mathbf{k}_{ex}}}{2} |K', \mathbf{k}_{ex}\rangle$ , as a Bloch vector in terms of the geometrical angles  $\theta_{S, \mathbf{k}_{ex}}$  and  $\phi_{S, \mathbf{k}_{ex}}$ , allowing for visualization in the Bloch sphere (see Supplementary Materials [32] for details). Figure 4a presents the Bloch vectors of the lowest spin-like exciton states over the BZ forming a valley-pseudospin texture. Around the  $\Gamma_{ex}$ -point, the phase angle  $\phi_{S, \mathbf{k}_{ex}}$  as a function of  $\mathbf{k}_{ex}$  is evolved with rotating  $\mathbf{k}_{ex}$  with a winding number  $n_w = 2$ , reflecting the dipole-dipole interacting nature of the  $e$ - $h$  exchange interaction. [4, 13, 38] Sustained by the symmetries, the valley pseudo-spin texture of the full-zone exciton band in the momentum space is anisotropically patterned by individual skyrmion-like structures centred with highly valley-polarized exciton states in the  $Q_{ex, i}/Q'_{ex, i}$  and  $K_{ex}/K'_{ex}$  excitonic valleys. In spite of the violation of the momentum selection rules, those inter-valley exciton states inherited with the high degree of valley polarization could emit light via the two-step transition processes with the involvement of phonon- or defect-scattering. Experimentally, the indirect PLs from the lowest inter-valley exciton states with  $\mathbf{k}_{ex} \in K_{ex}/K'_{ex}$  have been recently observed and, interestingly, present superiorly high optical polarization. [14–16]

Considering the phonon and photon reservoirs and their couplings to excitons, the total Hamiltonian of the extended exciton-photon-phonon system reads  $H = H_X + H_\nu + H_{ph} + H_{X-\nu} + H_{X-ph}$ , where  $H_X = \sum_{S, \mathbf{k}_{ex}} E_{S, \mathbf{k}_{ex}}^X \hat{X}_{S, \mathbf{k}_{ex}}^\dagger \hat{X}_{S, \mathbf{k}_{ex}}$  stands for the single-exciton Hamiltonian,  $\hat{X}$  ( $\hat{X}^\dagger$ ) is the operator annihilating (creating) an exciton and  $H_\nu = \sum_{\epsilon} \sum_{\mathbf{k}_\nu} \hbar \omega_{\mathbf{k}_\nu}^\epsilon a_{\epsilon, \mathbf{k}_\nu}^\dagger a_{\epsilon, \mathbf{k}_\nu}$  ( $H_{ph} = \sum_{\lambda} \sum_{\mathbf{q}} \hbar \Omega_{\mathbf{q}}^\lambda b_{\lambda, \mathbf{q}}^\dagger b_{\lambda, \mathbf{q}}$ ) is the Hamiltonian of photon (phonon) reservoir, where  $\omega_{\mathbf{k}_\nu}^\epsilon$  is the frequency of the  $\epsilon$ -polarized photon with the wave vector  $\mathbf{k}_\nu$  and  $a$  ( $a^\dagger$ ) is the particle operator that annihilates (creates) the photon,  $\Omega_{\mathbf{q}}^\lambda$  is the frequency of the  $\lambda$ -kind of phonon with the wave vector  $\mathbf{q}$ , and  $b$  ( $b^\dagger$ ) is the particle operator that annihilates (creates) the phonon.  $H_{X-\nu}$  ( $H_{X-ph}$ ) is the Hamiltonian of exciton-photon (exciton-phonon) coupling in terms of the coupling constants  $\eta_{S, \mathbf{k}_{ex}} (g_{S', \mathbf{k}'_{ex}; S, \mathbf{k}_{ex}})$  that converts an exciton in the bright state  $|S, \mathbf{k}_{ex}\rangle$  to a photon (that couples the exciton states  $|S, \mathbf{k}_{ex}\rangle$  and  $|S', \mathbf{k}'_{ex}\rangle$ ). The complete formalisms of  $H_{X-\nu}$  and  $H_{X-ph}$  are explicitly provided in Supplementary Material [32].



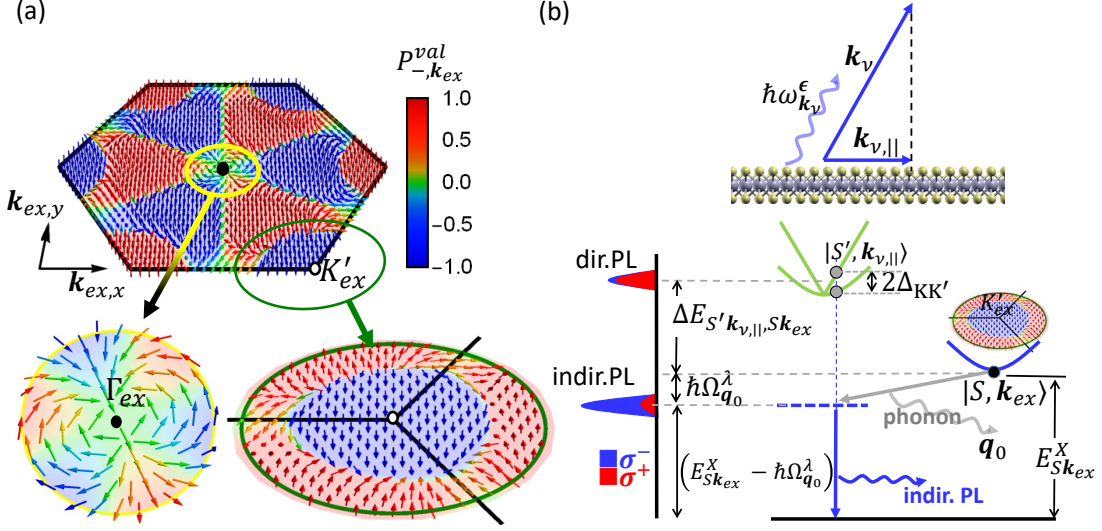


FIG. 4: (a) Valley-pseudospin texture of the valley-polarized exciton states over the entire BZ. Left (Right) inset: Zoom-in view of the pseudospin texture around the  $\Gamma_{ex}$  ( $K'_{ex}$ ) point. (b) Schematics of a phonon-assisted indirect PL process. The upper inset depicts the non-vertically emitted light with  $\mathbf{k}_{\nu,||} \neq \mathbf{0}$  from an indirect PL, in coincidence with the wave vector of the intermediate bright states  $|S', \mathbf{k}_{ex} = \mathbf{k}_{\nu,||}\rangle$ .

From the second-order perturbation theory, the transition rate of the phonon-assisted PL is evaluated by

$$\Gamma_{f \leftarrow i}^{(2)} = \frac{2\pi}{\hbar} \left| \sum_m \frac{\langle f | \hat{H}_{X-\nu} | m \rangle \langle m | \hat{H}_{X-ph} | i \rangle}{E_i - E_m + i0^+} \right|^2 \delta(E_f - E_i), \quad (3)$$

where  $|i\rangle$  denotes the initial state,  $|m\rangle$  the intermediate states following the emission or absorption of a phonon, and  $|f\rangle$  is the final state of the indirect PL. Specifically, we shall evaluate the transition rate of the indirect PL emitting the photons with a given wave vector  $\mathbf{k}_\nu$  from some exciton initial state,  $|S, \mathbf{k}_{ex}\rangle$ . In the situation, the wave vectors of the intermediate bright exciton states,  $|S', \mathbf{k}'_{ex}\rangle$ , and the phonons really involved in the transition process are deterministic under the law of momentum conservation, i.e.  $\mathbf{k}'_{ex} = \mathbf{k}_{\nu,||}$  and  $\mathbf{q} = \mathbf{k}_{ex} - \mathbf{k}_{\nu,||} \equiv \mathbf{q}_0$ , as illustrated in Fig. 4b.

Considering a valley-mixed initial state,  $|S, \mathbf{k}_{ex}\rangle = \alpha_{S, \mathbf{k}_{ex}}^K |K, \mathbf{k}_{ex}\rangle + \alpha_{S, \mathbf{k}_{ex}}^{K'} |K', \mathbf{k}_{ex}\rangle$ , the transition rates of the  $\sigma^+$ - and  $\sigma^-$ -polarized indirect PL's via the intermediate bright exciton doublet,  $|\pm, \mathbf{k}_{\nu,||}\rangle$ , split by  $2|\tilde{\Delta}_{KK'}(\mathbf{k}_{\nu,||})|$  are derived as  $\Gamma_{S, \mathbf{k}_{ex}}^{(2)}(\sigma^\pm) \approx$

$\gamma_0^{(2)} \left| \alpha_{S, \mathbf{k}_{ex}}^{K_{\pm}} + \tilde{\beta}_{\mathbf{k}_{\nu, \parallel}}^{K_{\pm} K_{\mp}} \alpha_{S, \mathbf{k}_{ex}}^{K_{\mp}} \right|^2 \times \delta \left( E_{S, \mathbf{k}_{ex}}^X - \hbar \Omega_{q_0}^{\lambda} - \hbar \omega_{\mathbf{k}_{\nu}}^{\epsilon} \right)$ , where the symbol  $K_+$  ( $K_-$ ) are introduced to denote the  $K$ - ( $K'$ )-valley,  $\gamma_0^{(2)}$  is the averaged transition rate of the polarization-unresolved indirect PL,  $\tilde{\beta}_{\mathbf{k}_{\nu, \parallel}}^{K_{\pm} K_{\mp}} \approx -\frac{\tilde{\Delta}_{K_{\pm} K_{\mp}}(\mathbf{k}_{\nu, \parallel})}{\Delta E_{-, \mathbf{k}_{\nu, \parallel}; S, \mathbf{k}_{ex}} + \hbar \Omega_{q_0}^{\lambda}}$ ,  $\tilde{\Delta}_{K_{\pm} K_{\mp}}$  is the matrix element of  $e$ - $h$  exchange interaction that couples the  $K_{\pm}$ - and  $K_{\mp}$ -valley exciton and  $\Delta E_{-, \mathbf{k}_{\nu, \parallel}; S, \mathbf{k}_{ex}} \equiv E_{-, \mathbf{k}_{\nu, \parallel}}^X - E_{S, \mathbf{k}_{ex}}^X$ . Accordingly, one can show that the optical polarization, defined by  $P_{S, \mathbf{k}_{ex}}^{op(2)} \equiv \frac{\Gamma_{S, \mathbf{k}_{ex}}^{(2)}(\sigma^+) - \Gamma_{S, \mathbf{k}_{ex}}^{(2)}(\sigma^-)}{\Gamma_{S, \mathbf{k}_{ex}}^{(2)}(\sigma^+) + \Gamma_{S, \mathbf{k}_{ex}}^{(2)}(\sigma^-)}$ , of the indirect PL from  $|S, \mathbf{k}_{ex}\rangle$  is given by [32]

$$P_{S, \mathbf{k}_{ex}}^{op(2)} \approx P_{S, \mathbf{k}_{ex}}^{val} \left( 1 - 4 \Re \left[ \tilde{\beta}_{\mathbf{k}_{\nu, \parallel}}^{KK'} (\alpha_{S, \mathbf{k}_{ex}}^K)^* \alpha_{S, \mathbf{k}_{ex}}^{K'} \right] \right), \quad (4)$$

which accounts for the degree of conversion of the valley-polarization of an inter-valley exciton to the optical polarization of the resulting indirect PL. For WSe<sub>2</sub>-ML's,  $|\tilde{\Delta}_{KK'}(\mathbf{k}_{\nu, \parallel})| \sim 1\text{meV}$  [13] and  $(\Delta E_{-, \mathbf{k}_{\nu, \parallel}; S, \mathbf{k}_{ex}} + \hbar \Omega_{q_0}^{\lambda}) \sim 60\text{meV}$ . [14, 15, 39] The latter is measurable from the energy difference between the direct and indirect PLs from bright exciton and inter-valley one, [14, 15, 39] respectively, as illustrated by Fig. 4b. Accordingly, one can estimate  $|\tilde{\beta}_{\mathbf{k}_{\nu, \parallel}}^{KK'}| \ll 0.1$ , with which the optical polarization of the indirect PL is thus shown nearly the same as the degree of valley polarization of the initial inter-valley exciton state according to Eq. 4. Note that the effect of valley-depolarization from the intermediate bright states is naturally suppressed in a second-order PL process. As a result, the valley-polarization of the inter-valley exciton state is actually excellently well transferable to the resulting optical polarization. This might account for the recently observed highly polarized indirect PL from tungsten-based TMD-MLs. [14–16]

In conclusion, we present a theoretical and computational investigation of the complete full-zone exciton band structures of TMD-MLs. While the bright exciton states of TMD-MLs lying around the central of the BZ are known to be inherently valley-depolarized, our studies reveal that most finite-momentum exciton states over the BZ are actually well immune from the exchange-induced valley depolarization, except for those with specific exciton momenta directionally in coincident with the axes of  $C'_2$  and  $\sigma_v$  symmetries. Sustained by the symmetries of TMD-ML, the valley pseudo-spin texture of the exciton states over the entire BZ is locally featured by skyrmion-like structures surrounding the highly valley-polarized inter-valley states. Importantly, the superior valley polarizations of those inter-valley excitons are shown excellently transferable to the optical polarization under the assistance of phonons. The finding sheds light on the prospective of the valley-based photonics with the utilization

of those inter-valley finite momentum excitons.

P.Y.L. and S.J.C. thank M. Bieniek and P. Hawrylak for fruitful discussion. This study is supported by the Ministry of Science and Technology, Taiwan, under contracts, MOST 109-2639-E-009-001 and 109-2112-M-009 -018 -MY3, and by National Center for High-Performance Computing (NCHC), Taiwan.

- 
- [1] K. F. Mak, C. Lee, J. Hone, J. Shan, and T. F. Heinz, Phys. Rev. Lett. **105**, 136805 (2010), URL <https://link.aps.org/doi/10.1103/PhysRevLett.105.136805>.
  - [2] D. Xiao, G.-B. Liu, W. Feng, X. Xu, and W. Yao, Phys. Rev. Lett. **108**, 196802 (2012), URL <https://link.aps.org/doi/10.1103/PhysRevLett.108.196802>.
  - [3] X. Xu, W. Yao, D. Xiao, and T. F. Heinz, Nat. Phys. **10**, 343 (2014), URL <https://doi.org/10.1038/nphys2942>.
  - [4] H. Yu, G.-B. Liu, P. Gong, X. Xu, and W. Yao, Nat. Commun. **5**, 3876 (2014), URL <https://doi.org/10.1038/ncomms4876>.
  - [5] H. Zeng, J. Dai, W. Yao, D. Xiao, and X. Cui, Nat. Nanotech. **7**, 490 (2012), URL <https://doi.org/10.1038/nnano.2012.95>.
  - [6] K. F. Mak, D. Xiao, and J. Shan, Nat. Photon. **12**, 451 (2018), URL <https://doi.org/10.1038/s41566-018-0204-6>.
  - [7] G. Wang, A. Chernikov, M. M. Glazov, T. F. Heinz, X. Marie, T. Amand, and B. Urbaszek, Rev. Mod. Phys. **90**, 021001 (2015), URL <https://doi.org/10.1103/RevModPhys.90.021001>.
  - [8] T. Smoleński, M. Goryca, M. Koperski, C. Faugeras, T. Kazimierczuk, A. Bogucki, K. Nogajewski, P. Kossacki, and M. Potemski, Phys. Rev. X **6**, 021024 (2016), URL <https://doi.org/10.1103/PhysRevX.6.021024>.
  - [9] T. Yu and M. W. Wu, Phys. Rev. B **89**, 205303 (2014), URL <https://link.aps.org/doi/10.1103/PhysRevB.89.205303>.
  - [10] K. Hao, G. Moody, F. Wu, C. K. Dass, L. Xu, C.-H. Chen, L. Sun, M.-Y. Li, L.-J. Li, A. H. MacDonald, et al., Nat. Phys. **12**, 677 (2016), URL <https://doi.org/10.1038/nphys3674>.
  - [11] G. Wang, L. Bouet, D. Lagarde, M. Vidal, A. Balocchi, T. Amand, X. Marie, and B. Urbaszek, Phys. Rev. B **90**, 075413 (2014), URL <https://doi.org/10.1103/PhysRevB.90.075413>.

- [12] M. Glazov, E. Ivchenko, G. Wang, T. Amand, X. Marie, B. Urbaszek, and B. Liu, Phys. Status Solidi (b) **252**, 2349 (2015).
- [13] D. Y. Qiu, T. Cao, and S. G. Louie, Phys. Rev. Lett. **115**, 176801 (2015), URL <https://link.aps.org/doi/10.1103/PhysRevLett.115.176801>.
- [14] Z. Li, T. Wang, C. Jin, Z. Lu, Z. Lian, Y. Meng, M. Blei, M. Gao, T. Taniguchi, K. Watanabe, et al., ACS Nano **13**, 14107 (2019), URL <https://doi.org/10.1021/acsnano.9b06682>.
- [15] E. Liu, J. van Baren, C.-T. Liang, T. Taniguchi, K. Watanabe, N. M. Gabor, Y.-C. Chang, and C. H. Lui, Phys. Rev. Lett. **124**, 196802 (2020), URL <https://link.aps.org/doi/10.1103/PhysRevLett.124.196802>.
- [16] M. He, P. Rivera, D. V. Tuan, N. P. Wilson, M. Yang, T. Taniguchi, K. Watanabe, J. Yan, D. G. Mandrus, H. Yu, et al., Nat. Commun. **11**, 618 (2020), URL <https://doi.org/10.1038/s41467-020-14472-0>.
- [17] S. Brem, A. Ekman, D. Christiansen, F. Katsch, M. Selig, C. Robert, X. Marie, B. Urbaszek, A. Knorr, and E. Malic, Nano Letters **20**, 2849 (2020), pMID: 32084315, URL <https://doi.org/10.1021/acs.nanolett.0c00633>.
- [18] E. Liu, J. van Baren, T. Taniguchi, K. Watanabe, Y.-C. Chang, and C. H. Lui, Phys. Rev. Research **1**, 032007 (2019), URL <https://link.aps.org/doi/10.1103/PhysRevResearch.1.032007>.
- [19] S.-Y. Chen, T. Goldstein, T. Taniguchi, K. Watanabe, and J. Yan, Nat. Commun. **9**, 3717 (2018).
- [20] L. Wu, Y. Chen, H. Zhou, and H. Zhu, ACS Nano **13**, 2341 (2019), pMID: 30715845, URL <https://doi.org/10.1021/acsnano.8b09059>.
- [21] A. Koitzsch, A.-S. Pawlik, C. Habenicht, T. Klaproth, R. Schuster, B. Büchner, and M. Knupfer, npj 2D Mater. Appl. **3**, 41 (2019), URL <https://doi.org/10.1038/s41699-019-0122-6>.
- [22] J. Hong, R. Senga, T. Pichler, and K. Suenaga, Phys. Rev. Lett. **124**, 087401 (2020), URL <https://link.aps.org/doi/10.1103/PhysRevLett.124.087401>.
- [23] F. Wu, F. Qu, and A. H. MacDonald, Phys. Rev. B **91**, 075310 (2015), URL <https://link.aps.org/doi/10.1103/PhysRevB.91.075310>.
- [24] T. Deilmann and K. S. Thygesen, 2D Materials **6**, 035003 (2019).
- [25] M. Bieniek, L. Szulakowska, and P. Hawrylak, Phys. Rev. B **101**, 125423 (2020).

- [26] L. J. Sham and T. M. Rice, Phys. Rev. **144**, 708 (1966), URL <https://link.aps.org/doi/10.1103/PhysRev.144.708>.
- [27] W. Hanke and L. J. Sham, Phys. Rev. B **21**, 4656 (1980), URL <https://link.aps.org/doi/10.1103/PhysRevB.21.4656>.
- [28] M. Rohlfing and S. G. Louie, Phys. Rev. Lett. **81**, 2312 (1998), URL <https://link.aps.org/doi/10.1103/PhysRevLett.81.2312>.
- [29] G.-H. Peng, P.-Y. Lo, W.-H. Li, Y.-C. Huang, Y.-H. Chen, C.-H. Lee, C.-K. Yang, and S.-J. Cheng, Nano Letters **19**, 2299 (2019), pMID: 30860847, URL <https://doi.org/10.1021/acs.nanolett.8b04786>.
- [30] L. V. Keldysh, JETP Lett. **29**, 658 (1979).
- [31] P. Cudazzo, I. V. Tokatly, and A. Rubio, Phys. Rev. B **84**, 085406 (2011), URL <https://link.aps.org/doi/10.1103/PhysRevB.84.085406>.
- [32] See Supplemental Material at <http://link.aps.org/supplemental/xxx/xxx>, which includes the details on the first principles computation, symmetry analysis, the establishment of pseudospin exciton model and the theory of phonon-assisted photoluminescence from inter-valley excitons.
- [33] G. Kresse and J. Furthmüller, Phys. Rev. B **54**, 11169 (1996), URL <https://link.aps.org/doi/10.1103/PhysRevB.54.11169>.
- [34] J. P. Perdew, K. Burke, and M. Ernzerhof, Phys. Rev. Lett. **77**, 3865 (1996), URL <https://link.aps.org/doi/10.1103/PhysRevLett.77.3865>.
- [35] D. Y. Qiu, F. H. da Jornada, and S. G. Louie, Phys. Rev. Lett. **111**, 216805 (2013), URL <https://link.aps.org/doi/10.1103/PhysRevLett.111.216805>.
- [36] A. Chernikov, T. C. Berkelbach, H. M. Hill, A. Rigosi, Y. Li, O. B. Aslan, D. R. Reichman, M. S. Hybertsen, and T. F. Heinz, Phys. Rev. Lett. **113**, 076802 (2014), URL <https://link.aps.org/doi/10.1103/PhysRevLett.113.076802>.
- [37] C. Robert, T. Amand, F. Cadiz, D. Lagarde, E. Courtade, M. Manca, T. Taniguchi, K. Watanabe, B. Urbaszek, and X. Marie, Phys. Rev. B **96**, 155423 (2017).
- [38] Z. Gong, W. Luo, Z. Jiang, and H. Fu, Scientific Reports **7**, 1 (2017).
- [39] S.-Y. Chen, M. Pieczarka, M. Wurdack, E. Estrecho, T. Taniguchi, K. Watanabe, J. Yan, E. A. Ostrovskaya, and M. S. Fuhrern, arXiv:2009.09602 [cond-mat.mes-hall] (2020).